Electronic Supplementary Information (ESI)

Horizontal lithium growth driven by surface dynamics on single crystal Cu(111) foil

Min-Ho Kim, Dong Yeon Kim, Yunqing Li, Juyoung Kim, Min Hyeok Kim, Jeongwoo Seo, Benjamin V. Cunning, Taewon Kim, Sang-Wook Park, Rodney S. Ruoff*, Dong-Hwa Seo*, Sunghwan Jin*, Hyun-Wook Lee*

*Corresponding authors. Email: rsruoff@ibs.re.kr, dseo@kaist.ac.kr, shjin00@kangwon.ac.kr, hyunwooklee@unist.ac.kr

This PDF file includes:

Other Supporting Online Material for this manuscript includes the following:

Notes

1. Large-scale production of single crystal Cu foils using contact-free annealing (CFA)

We prepared large-area single-crystal Cu(111) foil using contact-free annealing (CFA) from commercially available polycrystalline Cu foil[1] and used them as the substrate for *anode-free* lithium batteries, as illustrated in in Fig. 1 and Fig. S2, ESI†. During the CFA process, abnormal growth of the grain with the (111) surface (which has the lowest surface energy in FCC Cu) occurs to minimize the surface energy of the entire foil. As a result, we were able to routinely obtain large-area single-crystal Cu foil with approximate dimensions of 80 mm × 190 mm. In particular, it was reported that as-made Cu(111) foil has a very small misorientation angle (below 1^{o}) in all kernel average misorientation (KAM) maps, representing its 'perfect single crystallinity' in both the in-plane and normal directions.

While some previous studies used single crystal Cu substrates, these were commercially available single crystal sheets or plates that were produced by bulk crystal growth (*e.g.* Czochralski method) with a high material cost over $150 per square centimeter; also they are limited in lateral size. It is worth noting that a 'plate' generally exceeds 6 mm in thickness, a 'sheet' is more than 0.5 mm thick, while a 'foil' is less than 0.2 mm thick (and our foils used here are 0.05 mm thick). The sheet size is usually limited to the coin-cell size level due to their high cost, and their excessive thickness impedes the realization of high-energy density batteries. Our 0.05 mm thick single-crystal Cu(111) foil can be produced in large-areas using a simple annealing process, which allows for the straightforward construction of pouch-level cells (Fig. S22, ESI†). Therefore, with the high mass production capability, our Cu(111) foils open up the possibility of realizing commercial anode-free Li batteries in the near future.

2. Preparation of Cu(111) foil that contains twin boundary and grain with a (115) orientation

We made and used 'special' Cu(111) foil that contains some grains with a (115) surface orientation. During CFA, (115) grains (having a Σ3 twin relationship with respect to the (111) plane) are sometimes present in Cu(111) foil because of the formation of annealing twins [2]. The Cu(115) surface contains high-index facets, consisting of multiple (100) terraces and steps (Fig. 4a and Fig. S13). The (115) grains are easily distinguished using scanning electron microscopy (SEM) and optical microscopy (OM), as they have a rectangular shape and length of several micrometers and are well aligned with each other along the three-fold symmetry of the parent (111) plane.

3. Li dynamics on Cu(410) foil containing some (233) grains

We also experimentally investigated the Li dynamics on Cu(410) foil containing some (233) grains. The (233) grains in Cu(410) foil have a similar shape and size to the (115) grains in the Cu(111) foil because they are also annealing twins formed from the parent (410) grain. We found that the Li plating on the Cu(410) foil with (223) grains has plated Li 'crowded' on the

(410) region but ‘avoiding’ the (223) grains. As the (223) surface is close to the (111) surface, 3D plating of Li occurs preferentially on the (410) surface, possibly as a result of surface migration.

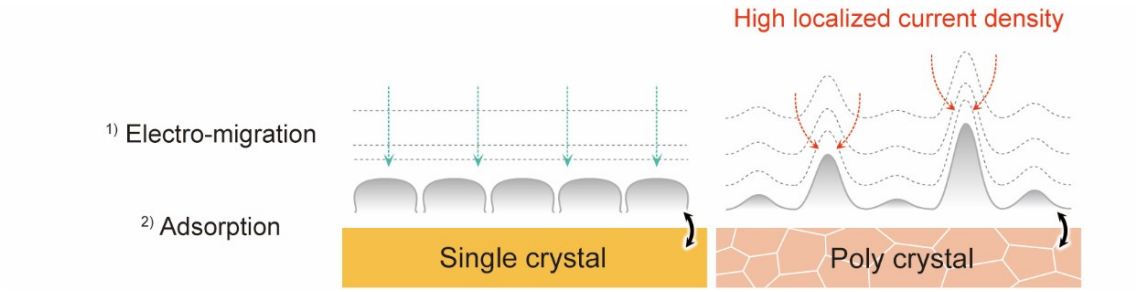

Fig. S1. Illustration of Li deposition on single crystal (left) and poly crystal Cu foil (right). Conventionally, it has been considered that Li deposition consists of electro-migration of Li ions in the electrolyte and Li adsorption onto the substrate. The Li ionic concentration gradient and uniformity of Li ionic flux can vary depending on the Li deposition chemistry.

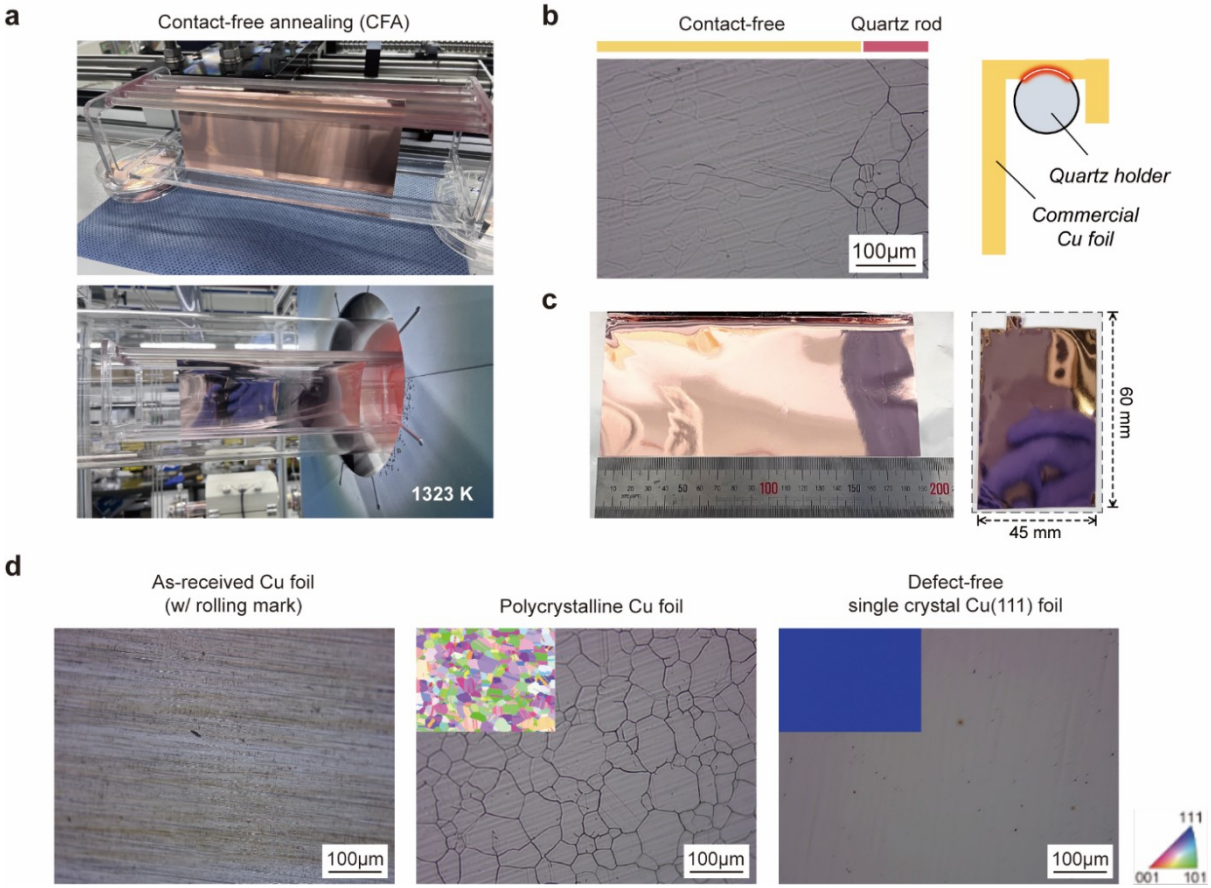

Fig. S2 The fabrication of large-sized single crystal Cu(111) foil via contact-free annealing. a, Contact-free annealing (CFA) process for the preparation of single crystal Cu(111) foil. Commercial polycrystalline Cu foil is suspended on the quartz holder, and annealed near the melting point of Cu. b, Optical microscopic image of an annealed folded Cu foil hung on a quartz holder. c, Digital photographs of as-prepared single crystal Cu(111) foil and slited Cu(111) foil. d, Microstructural evolution of as-received Cu foils during contact-free annealing. Upon annealing, the rolling marks of as-received Cu foils almost disappear and the size of grains increase. Annealed Cu foils contain a large number of grains with high-index facets until they are completely converted into single crystal Cu(111) foils. Insets are corresponding EBSD IPF maps.

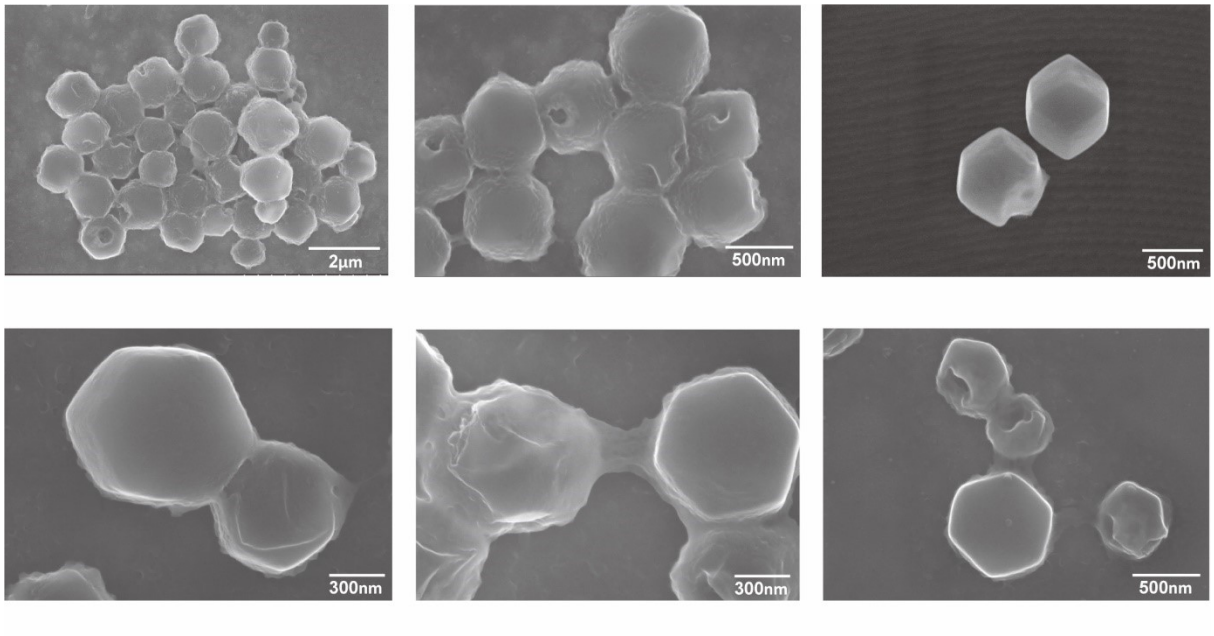

Fig. S3 Rhombic dodecahedral Li particles on Cu(111) foils formed after Li plating on single crystal Cu(111) with an areal capacity of 0.5 mAh cm^{-2} at a current density of 0.1 mA cm^{-2},.

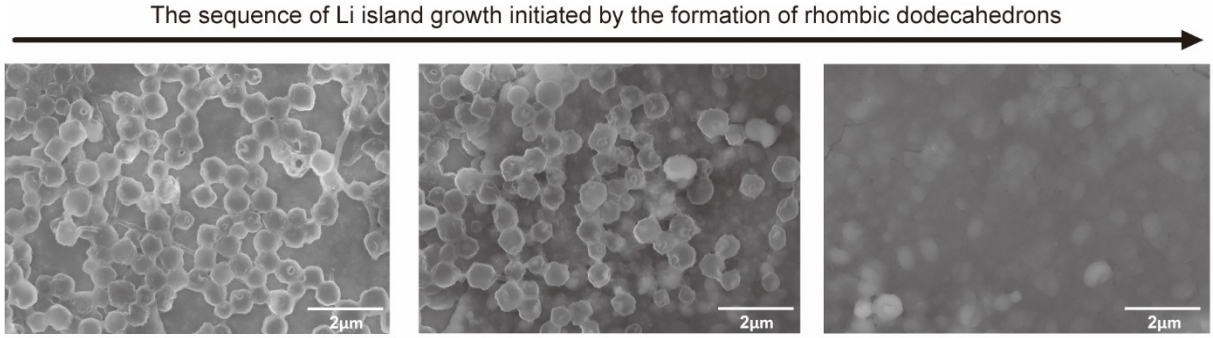

Fig. S4. The formation of Li island initiated by the formation of Li rhombic dodecahedron on Cu(111) surface. First, Li rhombic dodecahedra are formed. Then, these particles are covered by additional Li during subsequent plating, resulting in 2D growth of Li instead of dendritic growth of Li.

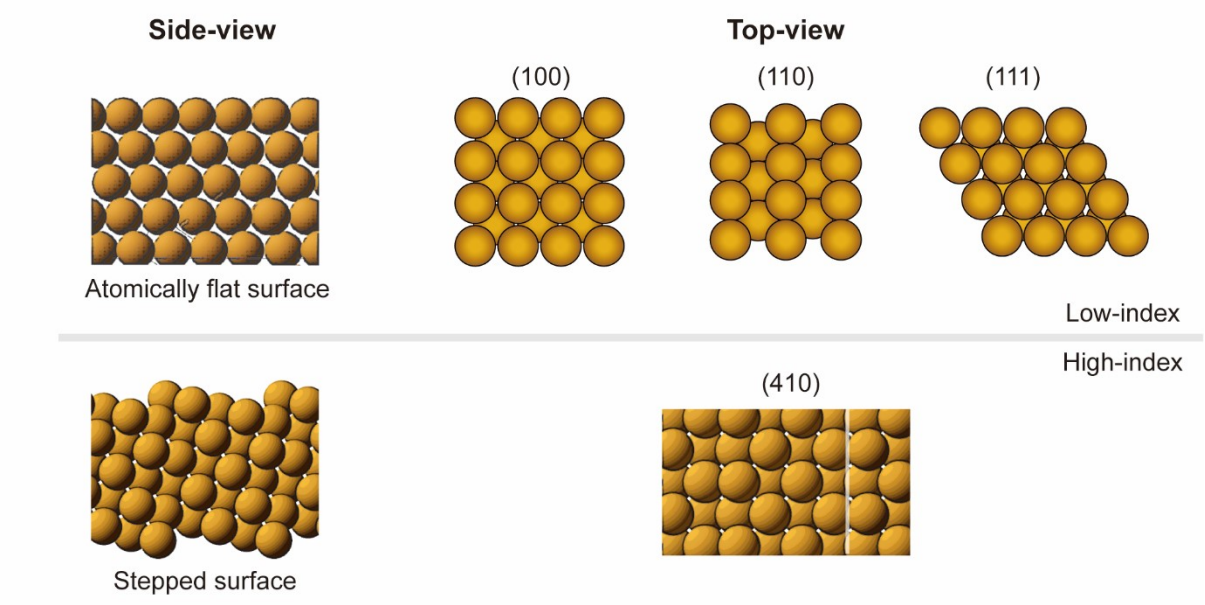

Fig. S5 Examples of model surfaces of Cu. Low-index surfaces (e.g., (100), (110), and (111)) have a flat and single surface, whereas high-index surfaces (e.g., (410)) has stepped surface, consisting of terrace, edge, and step sites.

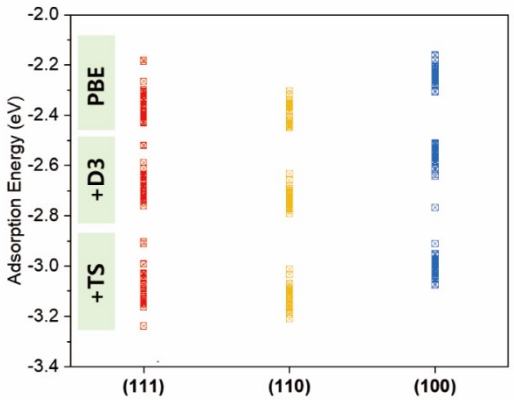

Surface energy (Cu)

Cu(111) < Cu(100) < Cu(110)

Interfacial energy (Li-Cu)

Cu(111) < Cu(110) < Cu(100)

Adsorption energy

Cu(111) < Cu(110) < Cu(100)

Fig. S6. DFT calculations of Li adsorption energies on low-index Cu surfaces.

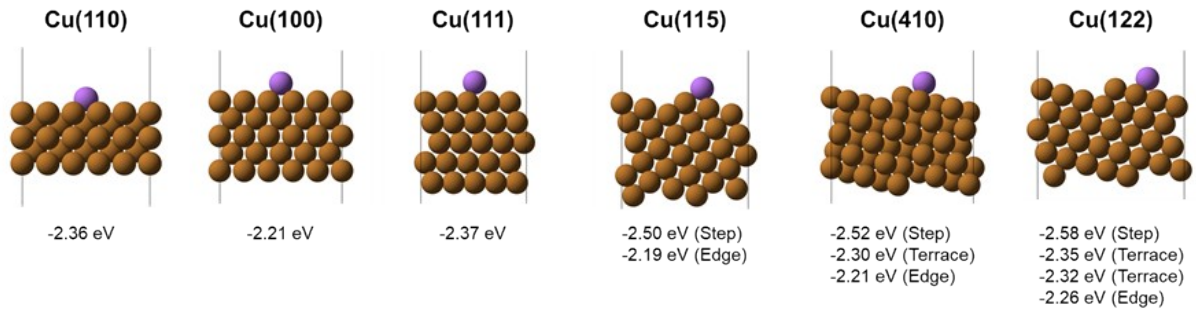

Fig. S7. Li adsorption energies for various low index ((110), (100), and (111)) and high index Cu facets ((115), (410), and (122)) based on first-principles calculations.

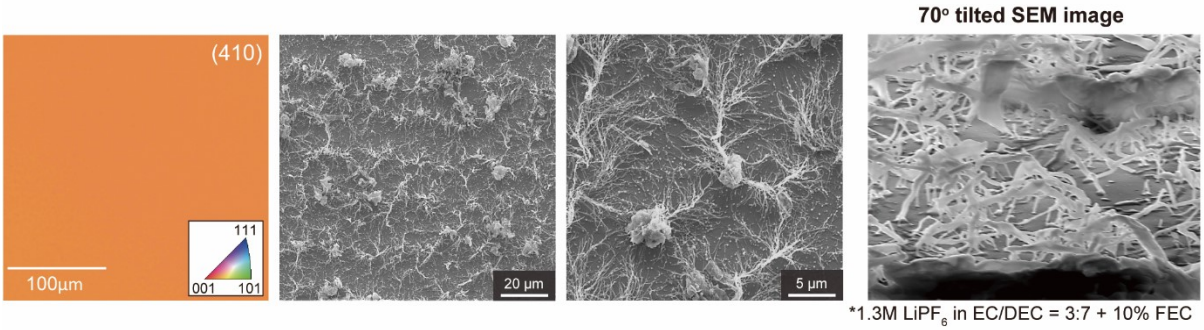

Fig. S8. Li deposition on the high-index Cu(410) foil. EBSD IPF map of single-crystal Cu(410) foil (left) and SEM images of Li electrodeposited on Cu(410) foil (right)

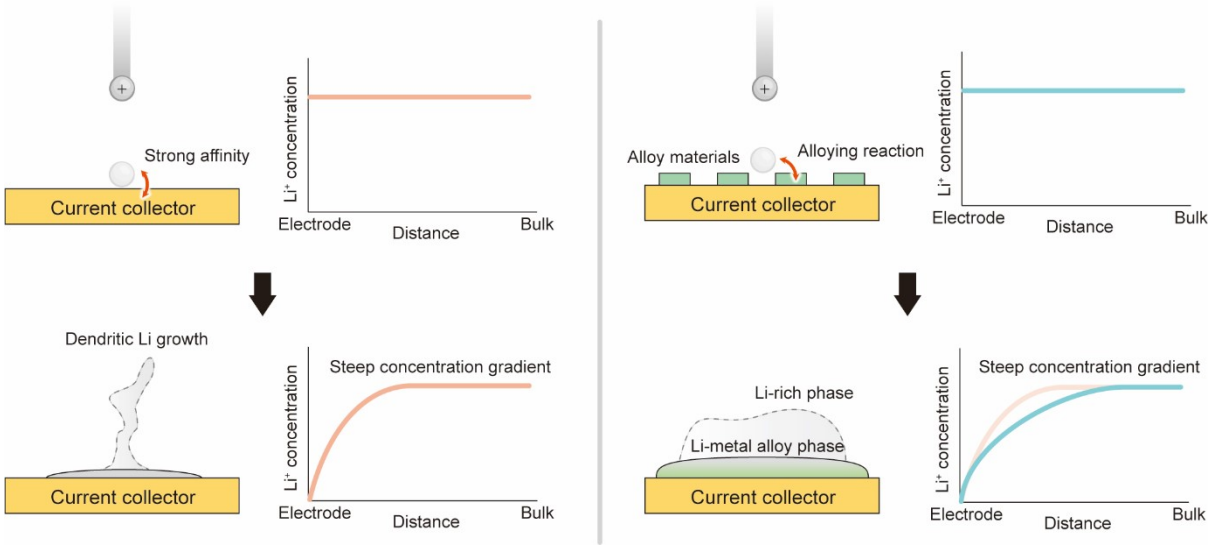

Fig. S9 Schematic illustrations of Li morphologies and corresponding concentration gradient on lithiophilic inert substrate (left) and substrate with alloy materials that can alloy with incoming Li (right).

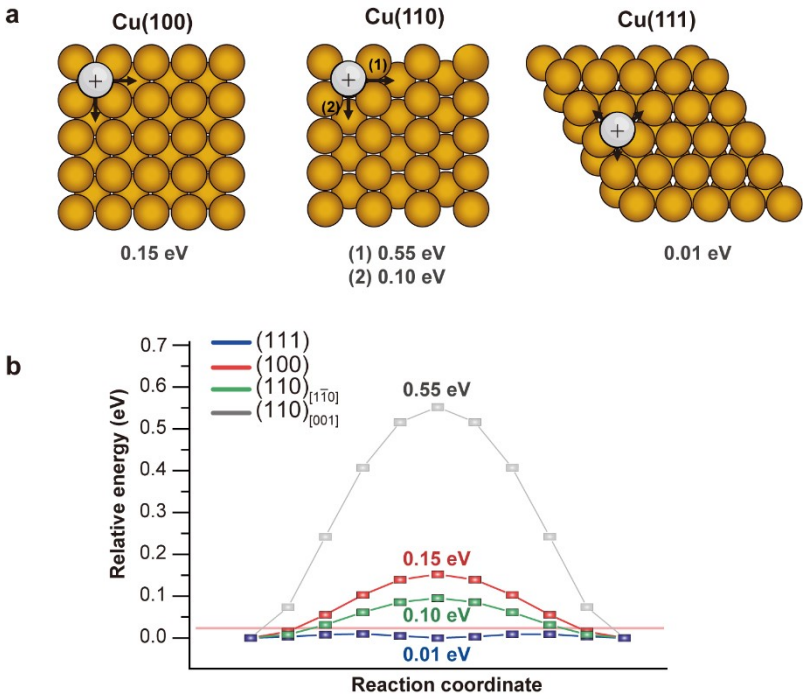

Fig. S10 Migration pathways (a) for Li adatoms and the corresponding energy barriers (b) on the Cu(110), Cu(100) and Cu(111) facets. The Cu(110) facet has two different energy barriers depending on its migration pathways, while the Cu(100) and Cu(111) facets each have one migration barrier.

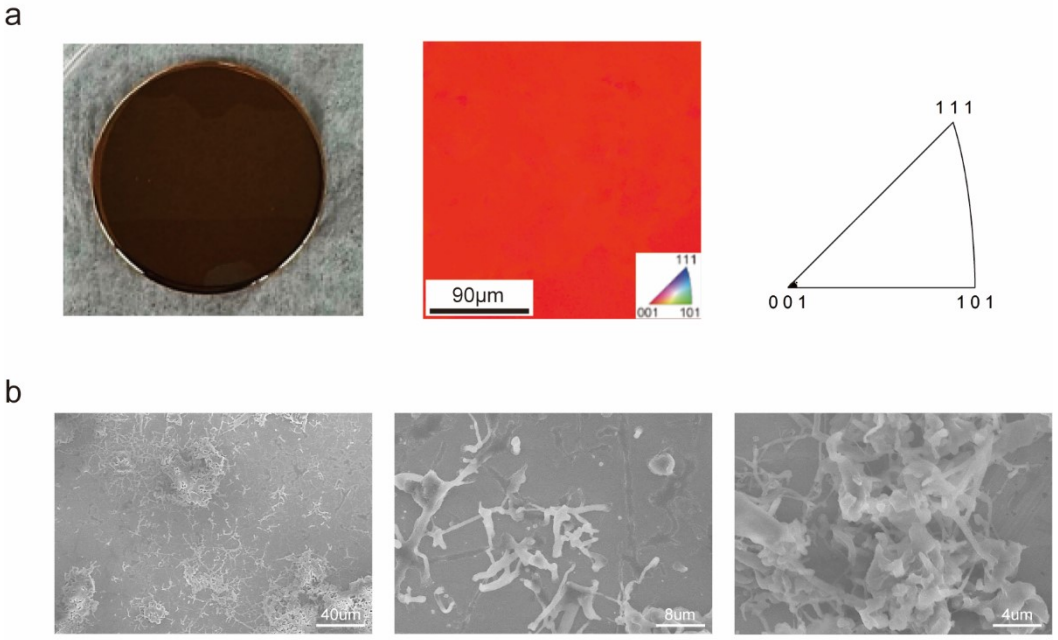

Fig. S11 Li deposition on single crystal Cu(100) sheet. (a) Characterization of single crystal Cu(100) sheet: digital photo and EBSD inverse pole figure (IPF) map. (b) Li deposition on Cu(100) sheet at 0.1 mA cm^{-2} for 30 min. 1.3M $LiPF_6$ in EC/DEC = 3:7 + 10% FEC was used as electrolyte system.

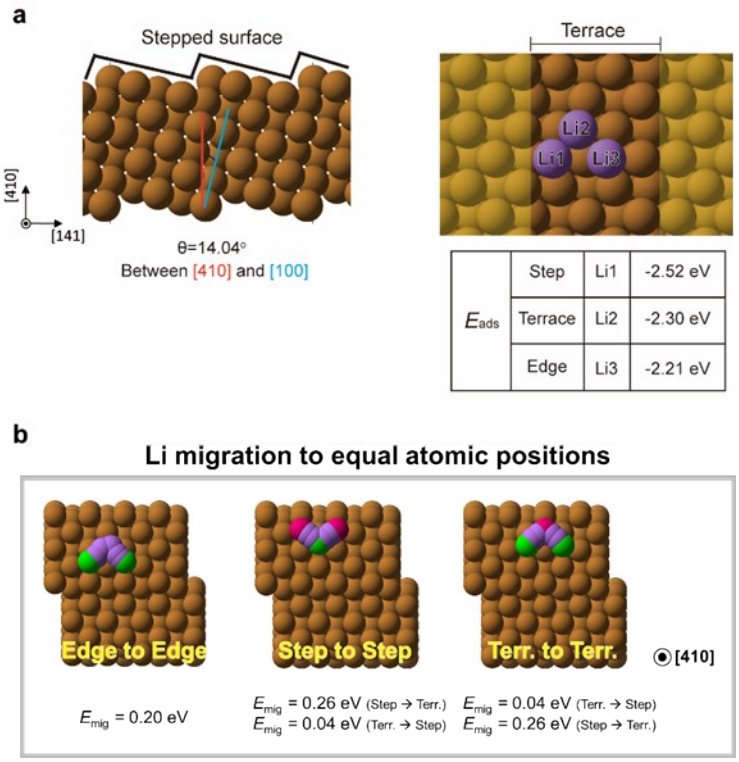

Fig. S12 Migration pathways for Li adatoms and the corresponding energy barriers on the Cu(410). a, Model structure of Cu(410) and DFT calculations of Li adsorption. Li adsorption energy depending on the adsorption sites (terrace and two different step sites) is -2.21 eV for edge, -2.30 eV for terrace, and -2.52 eV for the step, indicating Li is likely to preferentially be adsorbed on the step site. b, Activation barrier for Li migration is significantly lower for migration towards the steps than out of the steps or within equivalent positions, clarifying the Li is easy to be stuck on the step site.

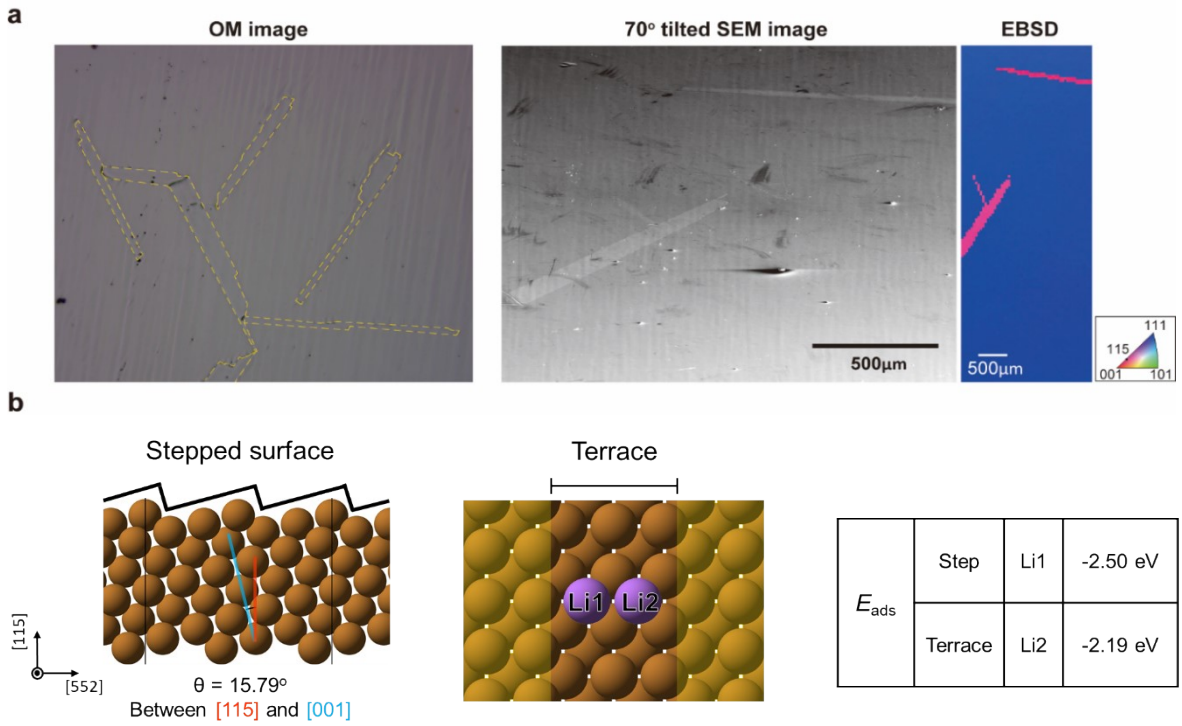

Fig. S13 (115) twin grains in Cu(111) foil. a, Observation results of twin grains: OM image (left), SEM image (middle), and EBSD IPF map (right). EBSD IPF map indicates the surface orientation of twin grains in Cu(111) foil is (115). b, DFT calculations of Li adsorption on Cu(115). The adsorption energy on step site of Cu(115) is much lower than that for Cu(111), suggesting that Li thermodynamically adsorbs onto (115) grain than (111) grain.

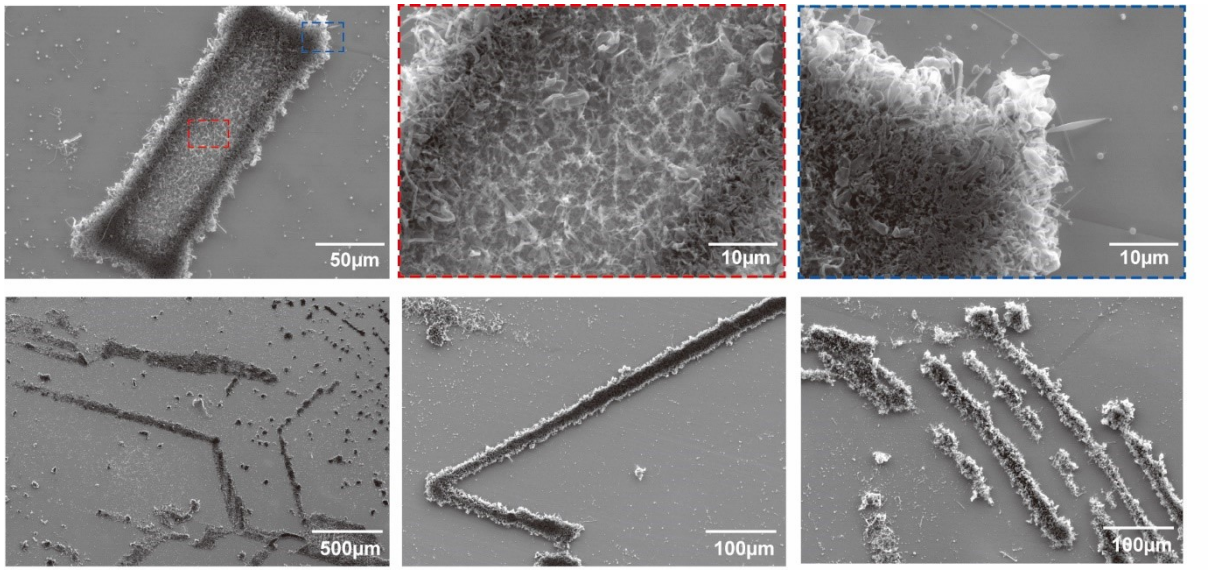

Fig. S14 (115) twin grains in Cu(111) foil and morphology of Li electrodeposited on the twin grains. Li deposits on (115) twin-containing Cu(111) foils, obtained from the conventional organic electrolyte system. There are two types of twin grains: Planar-type twin and Line-type twin. Regardless of the type of twins, Li is primarily deposited onto (115) grains before being plated on (111) grains, showing needle-like morphology.

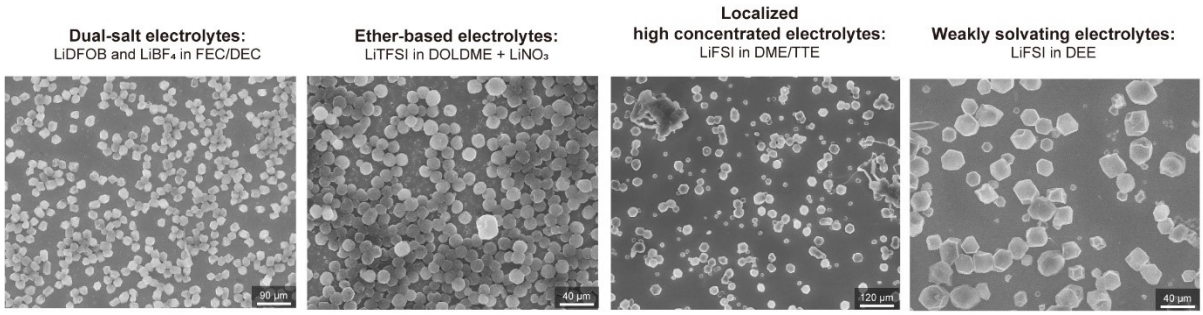

Fig. S15 Morphological analysis of electrodeposited Li on single crystal Cu(111) in dual-salt, ether-based, localized high concentrated, and weakly solvating electrolytes, showing rhombic dodecahedral Li growth regardless of the electrolyte systems.

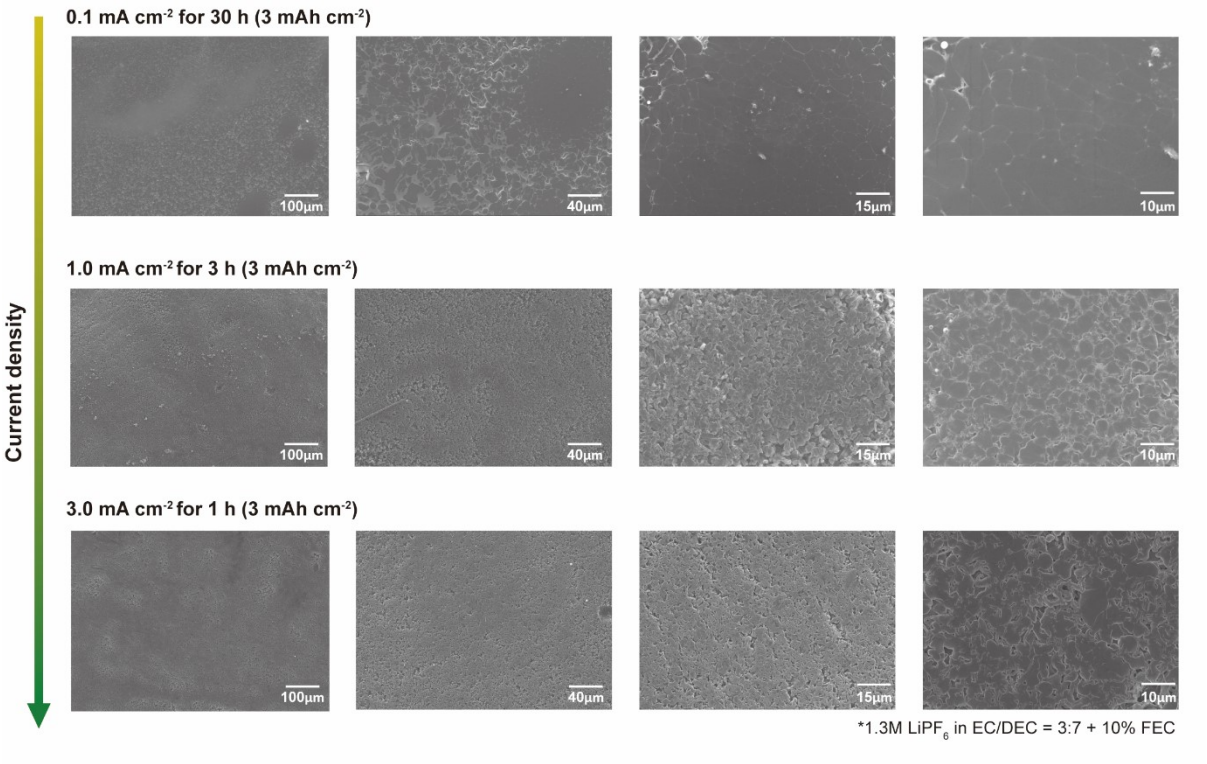

Fig. S16 SEM images of Li deposited on Cu(111) foils with different current densities. For all three deposition conditions the areal capacity was 3.00 mAh cm^{-2} and Li was deposited in a 2-dimensional (2D) manner.

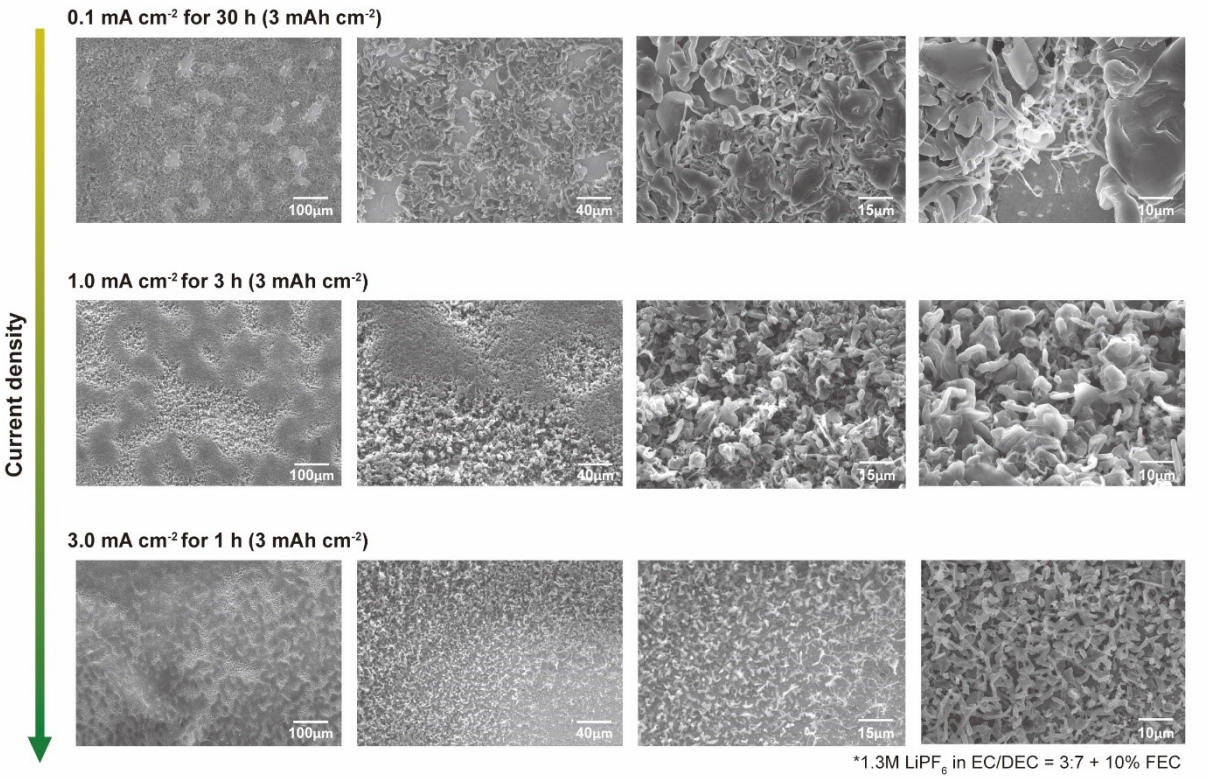

Fig. S17 SEM images of Li deposited on polycrystalline Cu foils with different current densities. For all three deposition conditions, the areal capacity was 3.00 mAh cm^{-2}**.** All Li deposits show a needle-like morphology. The higher the current density, the smaller the diameter of the needle-like Li deposits.

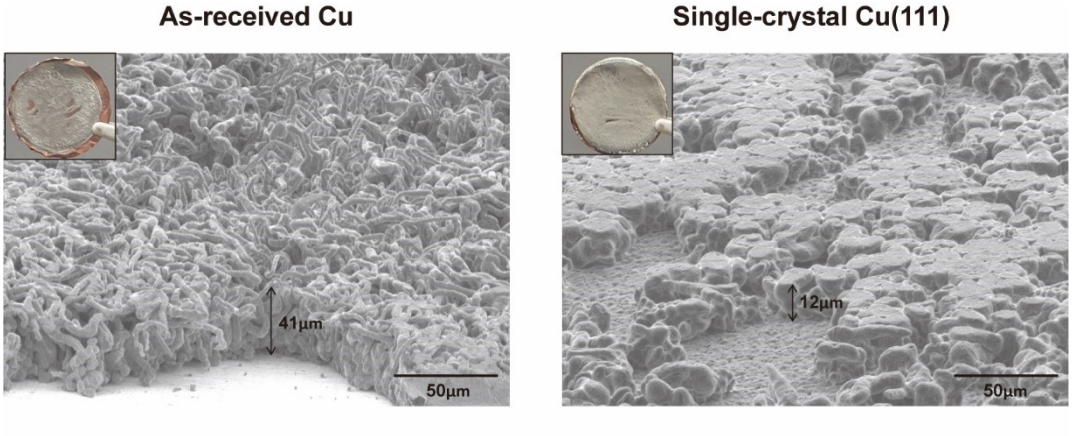

Fig. S18 SEM images (sample tilted at 70°) of Li deposited on as-received (polycrystalline) Cu versus Cu(111) foils at higher areal capacity (3.00 mAh cm^{-2}). Li was electrodeposited at a current density of 1.00 mA cm^{-2} in carbonate-based electrolyte systems. The insets are digital photographs of Cu foils after Li deposition. As-received Cu foils show rod-like Li deposits, while Cu(111) foils show disk-like Li deposits. Since Li is more homogeneously plated on Cu(111) foils than as-received Cu foils, as shown in these digital photographs, the typical height of Li on Cu(111) foils is at least 3 times lower than that on as-received Cu foils.

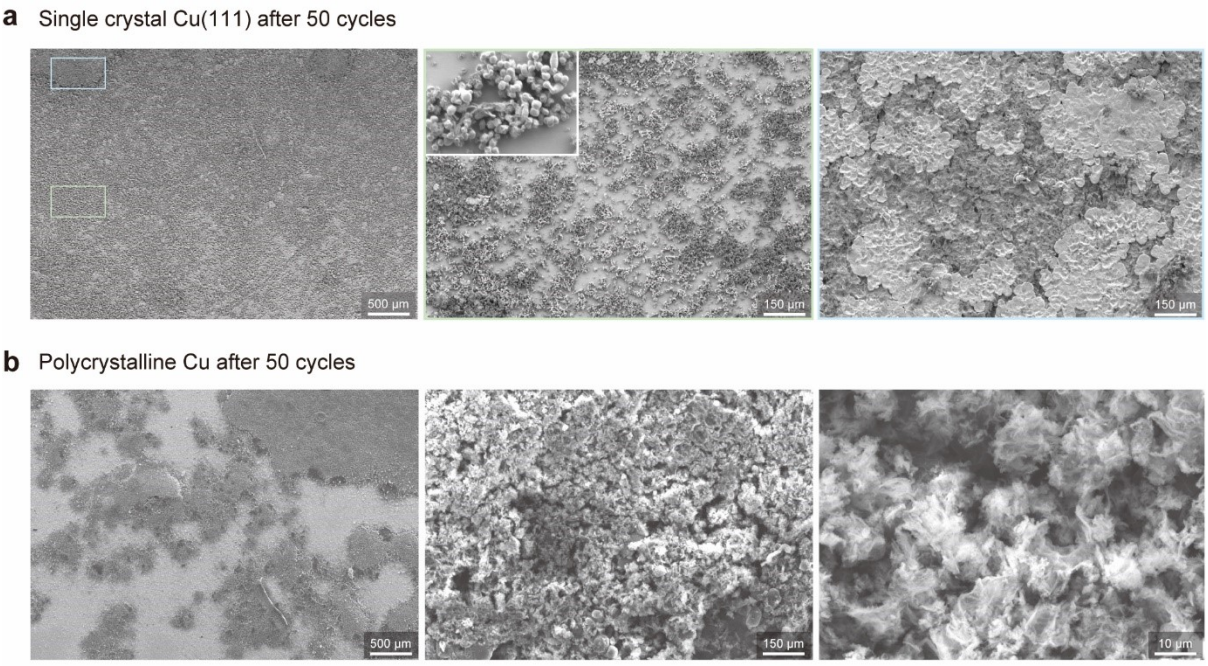

Fig. S19 SEM images of the residues on single crystal Cu(111) (a) and polycrystalline Cu foil (b) after 50 cycles.

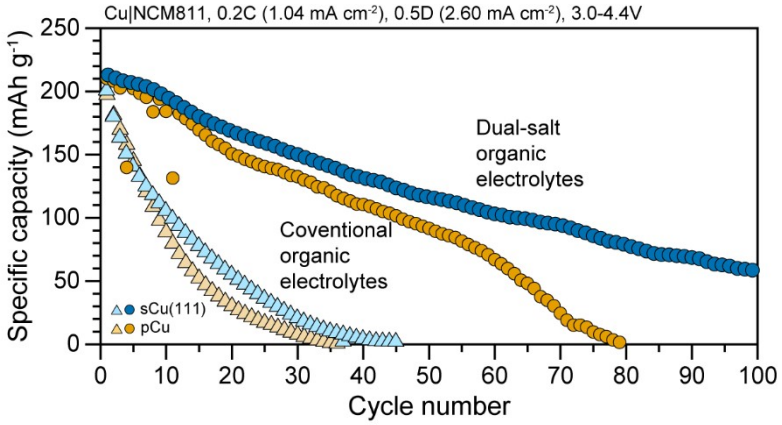

Fig. S20 Electrochemical performances of anode-free full-cells with NCM811 cathodes. Areal capacity of NCM811 electrode is 5.3 mAh cm^{-2}. Specific capacity versus cycle number of Cu|NCM811, operated at 0.2C (1.04 mA cm^{-2}) on charge and 0.5D (2.60 mA cm^{-2}) on discharge in 3.0-4.4 V, in conventional organic electrolyte (1.3 M $LiPF_6$ in EC/DEC = 3:7 v/v + 10 wt% FEC) and dual-salt organic electrolyte system (0.6 M LiDFOB and 0.6M $LiBF_4$ in FEC/DEC = 1:2 v/v).

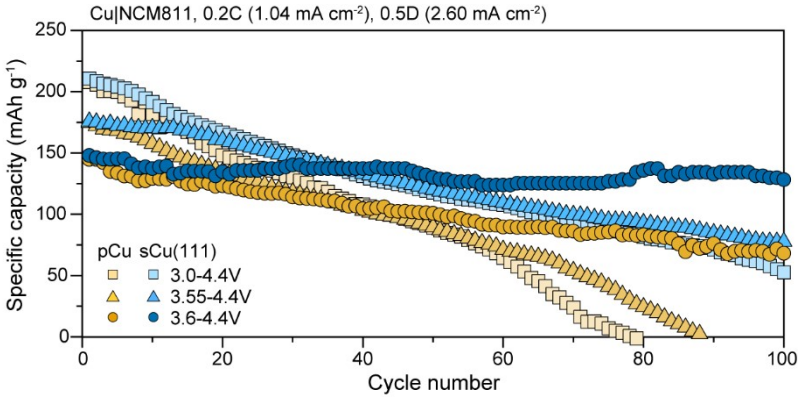

Fig. S21 Electrochemical performances of anode-free full-cells with NCM811 cathodes. Areal capacity of NCM811 electrode is 5.3 mAh cm^{-2}. Specific capacity versus cycle number of Cu|NCM811 cells at 0.2C and 0.5D, with different operating voltages (3.0-4.4 V, 3.55-4.4 V, and 3.6-4.4 V, corresponding to DOD95, DOD78, and DOD60, respectively).

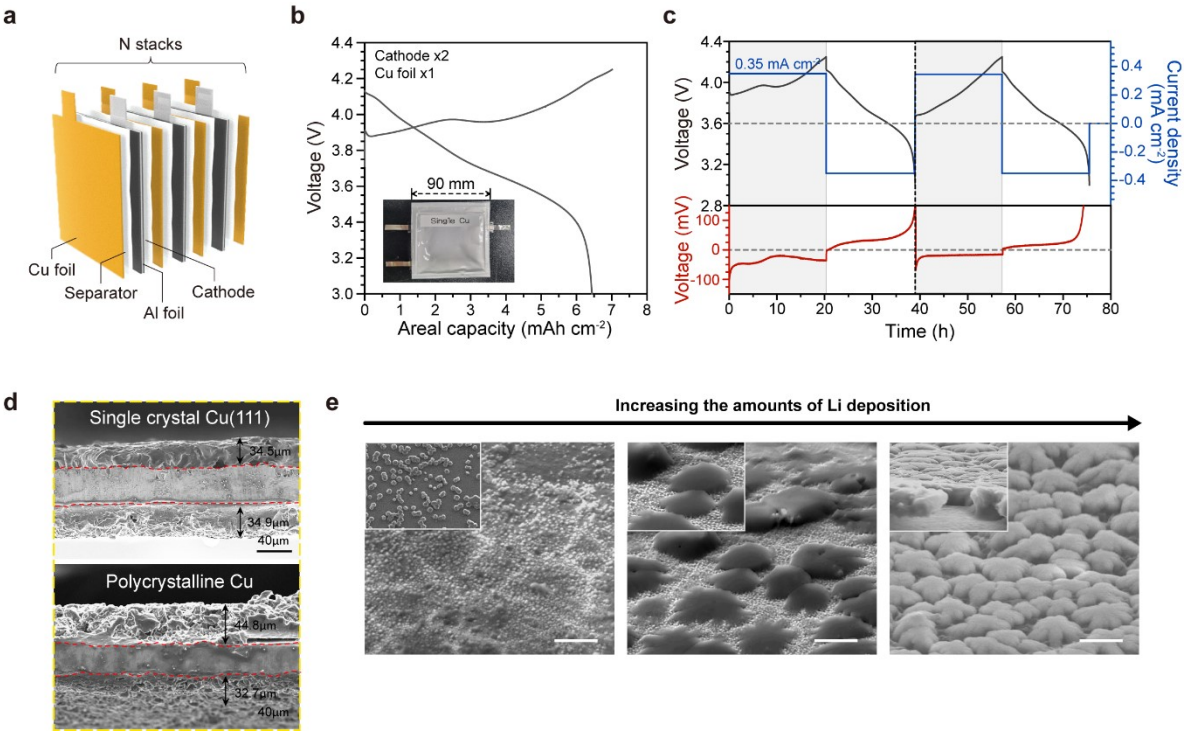

Fig. S22 Evolution of Li morphology in anode-free Li pouch cells. The cells consist of two NCM811 electrodes (working electrode, WE), a Cu foil (counter electrode, CE), and Li metal (reference electrode, RE) in conventional organic electrolyte system. a, Schematics of stacking pouch cell. b,c, Electrochemical characteristics of the Cu(111)|NCM811 pouch cell, which are plotted in a voltage–capacity graph (b) and voltage–time graph (c). As a current density of 0.35 mA cm^{-2} is applied, the cells show areal capacity of 7.0 mAh cm^{-2} in charge and 6.5 mAh cm^{-2} in discharge. The inset in (b) is a digital photograph of the stacking cell with an overall size of 90 mm × 90 mm. d, Cross-sectional SEM images of Li morphology deposited on Cu(111) and polycrystalline Cu foils after charging up to 4.25 V. e, Evolution of Li morphology with increasing the amounts of Li deposition.

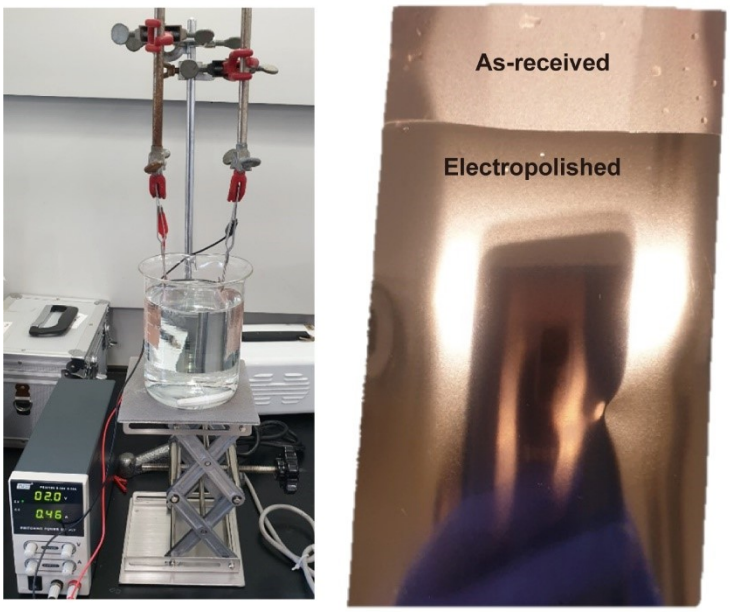

Fig. S23 Electropolishing of as-received polycrystalline Cu foil. Digital photographs of electropolishing setup (left) and electropolished Cu foil (right).

Table S1. Reports of Li plating depending on the crystallographic orientation of Cu substrates

No.	Substrate	Key findings	Notes
Our work	-Single crystal Cu(111) foil	-'Near zero' Li migration barrier on Cu(111) foil induces horizontal Li growth -Surface inhomogeneity in high index Cu surface (steps, edge, etc.) and grain boundaries prevent the Li migration, resulting in the dendritic Li growth	-Home-made perfect single-crystal Cu foil in large-area (size: **80 mm × 190 mm**)
[1][3]	-Single crystal Cu(111), (100), and (110) sheets -Poly Cu foil	-Li plating is most favored on the single crystal Cu (100) sheet since (100) surface has a lowest Li adsorption energy -Li is preferential deposited on (100) grains in the poly foil	**-Commercial single crystal sheets (size: 5 mm × 5mm)** **-Neglecting the 'grain with different orientations' and the 'grain boundaries present in the poly Cu foil.**
[2][4]	-(100)-dominant poly Cu foil and mesh	-The Cu(100) grain guides planar Li plating since Li(110) is lattice matched with it.	-**Neglecting the 'grain with different orientations' and the 'grain boundaries' present in the poly Cu foil.** -The effect of surface 'roughness' does not consider in the poly Cu mesh.
[3][5]	-Single crystal Cu(111), (100), (110) substrates	-The Cu(111) substrate forms thinnest solid electrolyte interphase (SEI) layer due to its lowest surface energy	**-Commercial single crystal substrates (no information for their dimensions)** **-**This work focuses on the SEI layer formation depending on the crystallographic orientations, **not on Li plating/stripping.**
[4][6]	-Nanosized Cu@MOF	-Nanosized Cu(100) and Cu(111) surfaces on MOF lead to a dense Li deposition on the 3D Cu_2O/C electrode owing to their lithiophilicity	-This work **does not explain Li dynamics on Cu substrates or yield practical Li batteries.**
[5][7]	-Single crystal Cu(110) substrate	-A lateral growth of Li on the single crystal Cu(110) substrate due to its homogeneous surface	**-Commercial single crystal substrates (no information for their dimensions)** -This work has insufficient evidence and logic to prove the electrochemical superiority of Cu(110). **According to them, other single crystal substrates should reach a similar result, but this is not true given the case of our single-crystal (410) foil.**
[6][8]	-(111)-preferred Cu foil and (111) nanotwinned Cu foil	-The twin boundaries in the (111) nanotwinned Cu foil have the lower interfacial energy than grain boundaries in (111)-preferred Cu foil, resulting in the more uniform Li deposits.	**-The presence of numerous nanoscale grain boundaries (and twin boundaries) in their foils makes it unclear to distinguish the effect of crystallographic orientation and grain boundaries on Li deposition**. **-As we discovered and explained, grain boundaries can trigger 3D Li plating, Indeed, their SEM images show vertical (or highly dendritic) Li growth.**

Captions for videos

Video S1. Optical video showing dendritic Li growth on polycrystalline Cu foil. During Li plating, Li continues to grow vertically toward dendritic Li without any migration. Scale bar, 10 μm.

Video S2. Optical video showing numerous Li particles on single crystal Cu(111) foil. Instead of dendritic Li growth, numerous Li particles are crowded and moving. Scale bar, 10 μm.

Video S3. Optical video showing active surface migration of a Li adatom. Scale bar, 50 μm.

Video S4. The Ab-initio molecular dynamics (AIMD) simulation results for Li dynamics on Cu(111) surface. Li adatoms (purple) freely moves in all directions. Li coverage for Cu facets is 0.5 (that is, Li atoms occupy a half of possible position on the Cu surface.

Video S5. The Ab-initio molecular dynamics (AIMD) simulation results for Li dynamics on Cu(100) surface. Li adatoms are trapped on its original sites. Li coverage for Cu facets is 0.5 (that is, Li atoms occupy a half of possible position on the Cu surface.

Video S6. The Ab-initio molecular dynamics (AIMD) simulation results for Li dynamics on Cu(110) surface. Li adatoms move along certain crystallographic direction. Li coverage for Cu facets is 0.5 (that is, Li atoms occupy a half of possible position on the Cu surface.

Video S7. The Ab-initio molecular dynamics (AIMD) simulation results for Li dynamics on Cu(410) surface. Li adatoms are trapped in step sites. After available step positions are fully occupied, other Li adatoms is favorable on terrace edge sites than terrace due to Li-Li repulsion. Li coverage for Cu facets is 0.5 (that is, Li atoms occupy a half of possible position on the Cu surface.

Video S8. Optical video showing preferential Li plating on Cu(115) over on Cu(111). Scale bar, 10 μm.

Video S9. The Ab-initio molecular dynamics (AIMD) simulation results for Li dynamics on a slab system consisting of (111) and (115) surfaces (top view). Upper and bottom regions correspond to (111) surface and middle region corresponds to (115) surface. Violet colored regions are grain boundaries between (111) and (115) surfaces, and green spheres are Li adatoms on the Cu surfaces. Li adatoms on the Cu(111) surfaces migrate freely until they are trapped on grain boundaries . On the other hand, Li adatoms on the Cu(111) surfaces were trapped on the step sites and did not migrate from these sites.

References

1. Jin, S. *et al.* Colossal grain growth yields single-crystal metal foils by contact-free annealing. *Science.* **362**, 1021–1025 (2018).

2. Bozzolo, N. & Bernacki, M. Viewpoint on the Formation and Evolution of Annealing Twins During Thermomechanical Processing of FCC Metals and Alloys. *Metall. Mater. Trans. A Phys. Metall. Mater. Sci.* **51**, 2665–2684 (2020).

3. Kim, Y.-J. *et al.* Facet selectivity of Cu current collector for Li electrodeposition. *Energy Storage Mater.* **19**, 154–162 (2019).

4. Gu, Y. *et al.* Lithiophilic Faceted Cu(100) Surfaces: High Utilization of Host Surface and Cavities for Lithium Metal Anodes. *Angew. Chemie Int. Ed.* **58**, 3092–3096 (2019).

5. Ishikawa, K., Harada, S., Tagawa, M. & Ujihara, T. Effect of Crystal Orientation of Cu Current Collectors on Cycling Stability of Li Metal Anodes. *ACS Appl. Mater. Interfaces* **12**, 9341–9346 (2020).

6. Qian, J. *et al.* Lithium Induced Nano-Sized Copper with Exposed Lithiophilic Surfaces to Achieve Dense Lithium Deposition for Lithium Metal Anode. *Adv. Funct. Mater.* **31**, 2006950 (2021).

7. Shen, C., Gu, J., Li, N., Peng, Z. & Xie, K. Single crystal Cu (110) inducing lateral growth of electrodeposition Li for dendrite-free Li metal-based batteries. *J. Power Sources* **501**, 229969 (2021).

8. Liu, S.-T., Ku, H.-Y., Huang, C.-L. & Hu, C.-C. Improvements in Li deposition and stripping induced by Cu (111) nanotwinned columnar grains. *Electrochim. Acta* **430**, 141011 (2022).